ACS MATERIALS Au
AN OPEN ACCESS JOURNAL OF THE AMERICAN CHEMICAL SOCIETY

pubs.acs.org/materialsau

Article

Microfluidic Production of Monodisperse Biopolymer Microcapsules for Latent Heat Storage

Takaichi Watanabe,* Yuko Sakai, Naomi Sugimori, Toshinori Ikeda, Masayuki Monzen, and Tsutomu Ono*

Cite This: *ACS Mater. Au* 2022, 2, 250–259

Read Online

ACCESS | Metrics & More | Article Recommendations | Supporting Information

ABSTRACT: Microencapsulation of phase change materials in a polymer shell is a promising technology to prevent them from leakage and to use them as a handleable powder state. However, the microencapsulation process is a time-consuming process because the typical shell-forming step requires polymerization or evaporation of the solvent. In this study, we report a simple and rapid flow process to prepare monodisperse biocompatible cellulose acetate (CA) microcapsules encapsulating *n*-hexadecane (HD) for latent heat storage applications. The microcapsules were prepared by combining microfluidic droplet formation and subsequent rapid solvent removal from the droplets by solvent diffusion. The diameter and shell thickness of the microcapsules could be controlled by adjusting the flow rate and the HD-to-CA weight ratio in the dispersed phase. We found that 1-hexadecanol added to the microcapsules played the role of a nucleation agent and mitigated the supercooling phenomenon during crystallization. Furthermore, cross-linking of the CA shell with poly(propylene glycol), tolylene 2,4-diisocyanate terminated, resulted in the formation of a thin and dense shell. The microcapsules exhibited a 66 wt % encapsulation efficiency and a 176 J g^{-1} latent heat storage capacity, with negligible supercooling. We believe that this microflow process can contribute to the preparation of environmentally friendly microcapsules for heat storage applications.

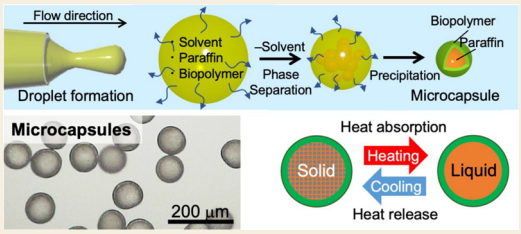

KEYWORDS: *microfluidics, phase separation, core–shell, cellulose acetate, latent heat storage*

INTRODUCTION

Phase change materials (PCMs) can absorb or release enormous energy when heated or cooled, thus maintaining a constant ambient temperature during the phase transition. In terms of industrial and dairy uses, microencapsulation of PCMs with a solid shell is a promising technology because it prevents leakage and evaporation of PCMs, and the smaller diameter increases the surface area-to-volume ratio, which improves the thermal conductivity.[1] Because of these advantages, PCM-encapsulated microcapsules have attracted much attention in thermal energy storage systems that collect thermal energy widely distributed in nature and human life and can mitigate the mismatch between energy supply and demand, which plays important roles in solving serious energy and environmental problems.

Microencapsulation of liquid oils has been performed by interfacial polymerization/polycondensation,[2−6] in situ polymerization,[7−9] suspension polymerization,[10−12] and emulsion polymerization.[13−15] Various types of shell materials have been used in these polymerization methods, including melamine-formaldehyde resin,[10,16,17] urea-formaldehyde resin,[18−22] polyurethane,[23,24] polystyrene,[25−27] and polyacrylates.[13,28−31] Another method for preparing microcapsules encapsulating PCMs is the phase separation method.[31] In this method, a droplet containing a shell polymer, PCMs, and their solvent is first formed, and then, the solvent is evaporated to induce phase separation between the polymer-rich and PCM-rich phases in the droplet; finally, PCM-encapsulated polymer microcapsules are formed. This method can be applied to synthetic polymers as well as bio-based polymers, including polylactide,[32,33] polycaprolactone,[34] and ethyl cellulose,[35,36] as shell materials. However, the solvent evaporation process is a time-consuming step that generally takes more than a few hours after droplet formation. Therefore, there is an increasing demand for the development of a simple and rapid process to produce microcapsules encapsulating PCMs.

In this study, we developed a simple and rapid flow process to prepare monodisperse bio-based polymer microcapsules encapsulating PCMs by combining microfluidic droplet formation with subsequent solvent diffusion.[33] In this method, a monodisperse droplet consisting of a polymer, a PCM (*n*-hexadecane, HD) and a solvent (methyl acetate, MA) was first formed in a microfluidic device, and the droplet was then carried by a continuous aqueous phase (water saturated with MA) to a large amount of the precipitation phase (pure water).

Received: November 1, 2021
Revised: December 27, 2021
Accepted: December 29, 2021
Published: January 26, 2022

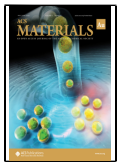

https://doi.org/10.1021/acsmaterialsau.1c00068
ACS Mater. Au 2022, 2, 250–259

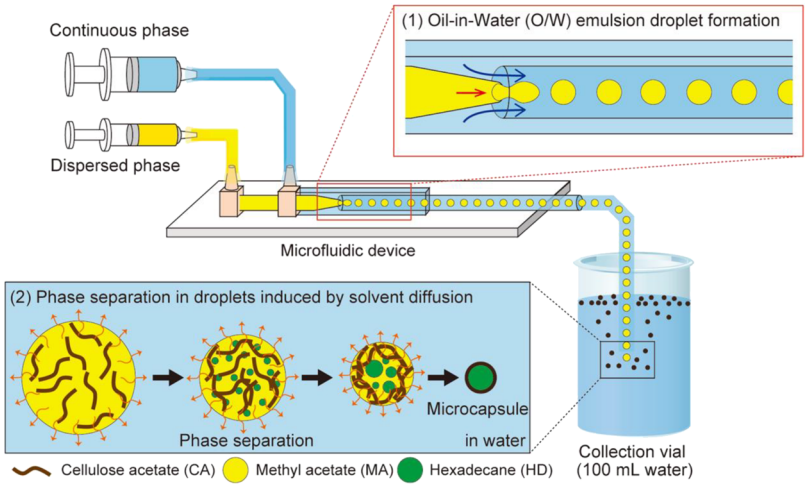

Figure 1. Schematic representation of a microflow process to produce cellulose acetate microcapsules encapsulating *n*-hexadecane.

In the precipitation phase, MA diffuses from the droplet into pure water, causing volume shrinkage of the droplet, internal phase separation of the polymer-rich and HD-rich phases, and precipitation of the polymer, finally resulting in polymer microcapsules encapsulating HD in the core. This microencapsulation process is simple because the microcapsules are obtained by simply feeding the dispersed and continuous phases consistently to a microfluidic device under ambient temperature and pressure. In addition, this process is a rapid microencapsulation method because microcapsules can be formed within a minute of droplet formation. In this study, cellulose acetate (CA) was employed as the shell material, which is a type of bio-based polymer with various advantages such as nontoxicity, low cost, easy degradation, good thermal and chemical stability, and high mechanical strength. To the best of our knowledge, this is the first report in which CA microcapsules encapsulating PCMs were prepared using a microflow process, and their latent heat storage properties were evaluated. Specifically, we first showed that monodisperse CA microcapsules encapsulating HD can be prepared using a microfluidic technology. Next, we evaluated the effects of the HD content in the microcapsules and the addition of 1-hexadecanol (HD-OH) as a nucleating reagent on the latent heat storage properties and morphology of the microcapsules. We then evaluated the effect of the cross-linking of the microcapsules on their shell structure and latent heat storage properties. Finally, we evaluated the thermal stability of the microcapsules by cyclic thermal tests to confirm their thermal reliability.

EXPERIMENTAL SECTION

Materials

All reagents were used as received. Cellulose acetate (CA) was purchased from Kanto Chemical Co., Inc., Japan. Methyl acetate (MA), 1-hexadecanol (HD-OH), and poly(vinyl alcohol) (PVA, DP = 1000, degree of saponification of 86−90 mol %) were purchased from FUJIFILM Wako Pure Chemical Corporation, Japan. Commercially available *n*-hexadecane (HD) was purchased from TCI, Japan. Poly(propylene glycol), tolylene 2,4-diisocyanate terminated (PPG-TDI, M_n = 2300), was purchased from Sigma-Aldrich, Japan. Distilled water with a resistance of 3 MΩ·cm was obtained by passing it through an Elix UV system.

Fabrication of the Microfluidic Device

To prepare oil-in-water (O/W) emulsions, a glass capillary microfluidic device was fabricated following a previous report[37] with some modifications. Using a puller (PC010, Narishige), a cylindrical glass capillary (Narishige; G-1, Japan) with a 0.6 mm inner diameter and a 1.0 mm outer diameter was heated and pulled to form a tapered tip with a 0.12 mm diameter. The collection capillary was a cylindrical glass capillary (Narishige; G-1, Japan), and the two capillaries were placed coaxially in a square glass capillary (VitroCom; cat. no. 8100, USA) with a 1.0 mm inner diameter. The glass capillary was fixed to a glass slide using an epoxy adhesive (Nichiban Araldite, Japan). A tube connector (1/16 inch, Index Health & Science, USA) was connected to the gap between the two square glass capillaries using an epoxy adhesive. All inlets of the microfluidic devices were connected to plastic disposable syringes (Henke Sass Wolf, Germany) via PTFE tubing (for 1/16 inch, GL Science, Japan). The outlet of the device was connected to a sampling vial via PTFE tubing (1/16-inch, GL Science, Japan). The syringe was set on a syringe pump (Harvard Apparatus 33DDS, USA) to precisely control the flow rate. The microfluidic device was placed on the stage of a digital microscope (VW-9000C, Keyence, Japan) equipped with a high-speed camera (VW-600C, Keyence, Japan).

Preparation of Microcapsules Encapsulating HD Using a Microfluidic System

In a dispersed oil phase, MA solutions containing (1) CA and HD (2:1, 1:1, and 1:2, w/w), (2) CA, HD, and HD-OH, or (3) CA, HD, HD-OH, and PPG-TDI were used. The concentration of CA in the solutions was fixed at 1 wt %. HD-OH was employed as a nucleating reagent, and its concentration was varied from 0 to 10 wt % relative to the amount of HD. PPG-TDI was used as a cross-linking reagent for CA, and its concentration was varied from 0 to 0.6 wt % relative to the amount of the dispersed phase. For a continuous aqueous phase, an aqueous solution containing 1 wt % PVA and a saturated amount of MA was used. Both the dispersed and continuous phases were filled into syringes and fed into the microfluidic device using a syringe pump (Harvard 33DDS, USA). Before injecting the dispersed phase, the microchannel was wetted with the continuous phase for a few minutes to prevent the dispersed phase from adhering to the microchannel wall during emulsification. The flow rates of the dispersed and continuous phases were set to 20 and 1000 μL min^{-1}, respectively. The dispersed and continuous phases were emulsified at the tip of the nozzle in the coaxial microfluidic device to continuously generate O/W emulsion droplets. The generated droplets were transferred through a PTFE tubing to a collection vial containing 100 mL of water (Figure 1). MA was then rapidly removed from the droplets into the water phase by solvent diffusion due to the high solubility of MA in water (25 wt % at 20 °C), and the CA

https://doi.org/10.1021/acsmaterialsau.1c00068
ACS Mater. Au 2022, 2, 250−259

microcapsules were precipitated. The microcapsules were washed three times with water through a filter paper (Advantec, no. 3, 70 mm in circumference) to separate the microcapsules from the liquid phase. For scanning electron microscopy (SEM) observation, the microcapsules were dried in a freeze dryer (FDU-1200, EYELA) overnight. For thermal analysis, the microcapsules were dried in an oven at 60 °C overnight.

Microscopy Observation of Droplets and Microcapsules

The formation of droplets was observed using a digital microscope (VW-9000C, Keyence, Japan) equipped with a high-speed camera (VW-600C, Keyence, Japan). The microcapsule dispersion was dropped on a glass slide before washing and observed under an optical microscope (BX53, OLYMPUS, Japan) with a digital camera. The morphology of the microcapsules after freeze-drying was observed using a scanning electron microscope (SEM, S-4700, Hitachi, Ltd., Japan) at magnifications of 1 or 2 kV. A sputter coater (E-1030, Ion Sputter, Hitachi, Ltd., Japan) was used to coat the samples with Pd−Pt to prevent charge-up. To prepare cross sections of the microcapsules, the lyophilized microcapsules were dispersed in a light-curing resin (Noland NOA81), and the dispersion of the samples was cured with UV light (λ = 365 nm) for several hours to ensure solidification of the resin. The resin was cut with a cutter to make a cross section of the microcapsules. The cross section was placed on a sample stage to observe the internal structure of the microcapsules using an SEM. Typically, the average diameter of the microcapsules was measured using 200 microcapsules from each sample. The shell thickness of the microcapsules was measured from at least 10 microcapsules in each sample.

FT-IR Analysis of Materials and Microcapsules

Fourier transform infrared (FT-IR) spectra of raw materials and microcapsules were measured using an FT-IR spectrometer (IRPrestige-21, Shimadzu, Japan). Neat CA, raw HD, raw TDI, microcapsules encapsulating HD, or cross-linked microcapsules encapsulating HD were mixed with KBr and pressed to a disk for measurement.

Thermal Properties of Microcapsules

The latent heat storage properties of the microcapsules were evaluated using a differential scanning calorimeter (DSC, TA7000, Hitachi High-Tech Corp., Japan) with nitrogen at a flow rate of 40 mL min^{-1} as the purge gas. In the typical measurement, a sample of approximately 10 mg was first cooled from 30 to −10 °C at a cooling rate of 1 °C min^{-1} and then heated to 30 °C at a heating rate of 1 °C min^{-1}. In the case of thermal cyclic tests, the cooling/heating rate was set at 5 °C min^{-1}, and the cyclic DSC measurement was performed 50 times to confirm the thermal stability of the microcapsules. The onset point of the crystallization (T_{oc}) or melting (T_{om}) was used as the phase change temperature. The latent heats (ΔH_c and ΔH_m) were calculated from the heating/cooling peak areas of the DSC thermogram. According to a previous report, ΔH^*_c and ΔH^*_m values were also given in units of Joules per 1 g of encapsulated HD (J (g HD)$^{-1}$).[28,38] These values were calculated from the following equation:

$$A = \left[\frac{B}{C}\right] \times 100 \tag{1}$$

where A is the ΔH^*_c and ΔH^*_m of the encapsulated HD in units of Joules per 1 g of encapsulated HD (J (g HD)$^{-1}$); B is the ΔH_c and ΔH_m of the encapsulated HD in units of Joules per 1 g (J (g capsule)$^{-1}$) obtained from the DSC thermogram; C is the HD content (wt %) obtained from the TGA thermogram.

The thermal stabilities of raw HD, neat CA, raw PPG-TDI, CA microcapsules encapsulating HD, and cross-linked CA microcapsules encapsulating HD were evaluated using a thermogravimetric/differential thermal analyzer (TG, DTG-60, Shimadzu Corp., Japan). Approximately 10 mg of the dried sample was placed on an alumina open pan on the TG stage, and the profile was recorded from room temperature to 500 °C at a heating rate of 10 °C min^{-1} in a nitrogen atmosphere. Before analysis, the samples were dried in an oven at 60 °C overnight.

RESULTS AND DISCUSSION

Prediction of the Equilibrium Structure of Droplets after Phase Separation

To prepare microcapsules consisting of a PCM (poor solvent) core and a polymer shell, the polymer shell is necessary to precipitate around the PCM core when the good solvent is removed by diffusion from droplets containing the PCM, shell polymer, and good solvent. It is well-known that the equilibrium structure of droplets after phase separation can be predicted based on the spreading coefficient theory[39] and can be controlled by the relative magnitude of the interfacial tension of the three phases, including the two organic phases and the aqueous (continuous) phase. In our system, CA, HD, MA, and an aqueous PVA solution saturated with MA were used as the polymer shell, core (poor solvent), good solvent, and continuous aqueous phase, respectively. Thus, theoretically, when droplets of two immiscible liquids (HD-rich and CA-rich phases) are brought into contact in the third immiscible liquid (continuous aqueous phase), the final equilibrium structure can be predicted by calculating the spreading coefficient values using the respective interfacial tensions. To obtain a core−shell structure after phase separation, the spreading coefficient S of each phase must satisfy the following conditions:

$$S_{C16} = \gamma_{CA-W} - (\gamma_{HD-W} + \gamma_{HD-CA}) < 0 \tag{2}$$

$$S_W = \gamma_{HD-CA} - (\gamma_{CA-W} + \gamma_{HD-W}) < 0 \tag{3}$$

$$S_{CA} = \gamma_{HD-W} - (\gamma_{HD-CA} + \gamma_{CA-W}) > 0 \tag{4}$$

where S_i is the spreading coefficient of phase i. γ_{CA-W} is the interfacial tension between the CA-rich and continuous aqueous phases. γ_{HD-W} is the interfacial tension between the HD-rich and continuous water phases. γ_{HD-CA} is the interfacial tension between the HD-rich and CA-rich phases. The interfacial tension between the oil and water phases was measured to confirm the equilibrium structure of the droplets after phase separation, as shown in Table 1. The interfacial tension between the HD-rich and CA-rich phases could not be measured due to the low interfacial tension. If the interfacial tension between the HD-rich and CA-rich phases (γ_{HD-CA}) is assumed to be much lower than that of the other interfaces, then the values of the spreading coefficient for this system satisfy $S_{C16} < 0$, $S_W < 0$, and $S_{CA} > 0$, as shown in Table 2. This indicates that the droplet after phase separation is in equilibrium with a core−shell structure (Figure 2).

Table 1. Interfacial Tensions of an Emulsion System

entry	interfacial tension [mN m^{-1}]
C_{16}-PVA/water (γ_{C16-W})	18.2
CA/MA-PVA/water (γ_{CA-W})	1.4
C_{16}-CA/MA (γ_{C16-CA})	NA[a]

[a]The interfacial tension of γ_{C16-CA} could not be measured owing to the low interfacial tension.

https://doi.org/10.1021/acsmaterialsau.1c00068
ACS Mater. Au 2022, 2, 250−259

Table 2. Spreading Coefficients of Each Interface of an Emulsion System

entry	spreading coefficient [mN m^{-1}]
S_{C16}	−16.8
S_W	−19.6
S_{CA}	16.8

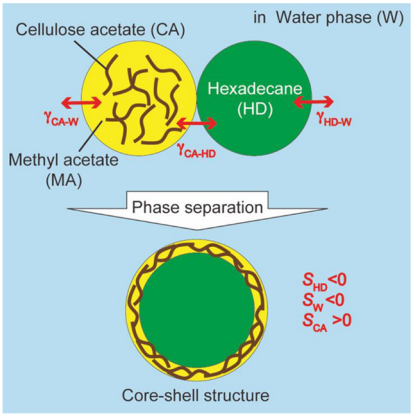

Figure 2. Schematic image of droplets with a core−shell structure after phase separation.

Preparation of Microcapsules Encapsulating PCMs Using a Microfluidic Device

To confirm the formation of CA microcapsules with a core−shell structure, CA microcapsules were prepared using a microfluidic platform. A polymer solution containing 1 wt % CA and 1 wt % HD and an MA-saturated aqueous solution containing 1 wt % PVA were injected into the glass capillary device as dispersed and continuous phases, respectively. The two phases merged at the exit of the inner nozzle to form O/W emulsion droplets owing to interfacial tension, as shown in Figure 3a. The droplets were then collected in a water coagulation bath, as shown in Figure 1. When the droplets were brought into contact with a large amount of water, MA began to diffuse from the droplets into the continuous aqueous phase because of the high solubility of MA in water (25 wt % at 20 °C). This solvent diffusion caused shrinkage of the droplets and phase separation between the CA/MA-rich and HD-rich phases in the droplets, resulting in the precipitation of CA and formation of microcapsules. The microcapsules floated on the air/water interface because of their lower density than water.

Optical microscopy observations revealed that the process yielded monodisperse CA microcapsules with a core−shell structure (Figure 3b). The diameter and coefficient of variation (CV) of the microcapsules were 88.3 μm and 4.3%, respectively, which indicates the narrow particle size distribution (Figure 3c). Some of the microcapsules were concave, but no observable shell rupture was confirmed. Figure 4 shows the representative FT-IR spectra of neat CA, raw HD, and CA microcapsules encapsulating HD. The spectrum of microcapsules encapsulating HD shows the typical characteristic bands for CA in the region of 3400−3600 cm^{-1} due to the absorption of the −OH group, at 2949 cm^{-1} due to the stretching vibration of the $-CH_2-$ group, at 1756 cm^{-1} due to the stretching vibration of the C═O group, and at 1431 cm^{-1} due to the bending vibration of the $-CH_2-$ group and those for HD at 2955, 2923, and 2853 cm^{-1} associated with the stretching vibrations of the C−H group and at 1470 and 1380

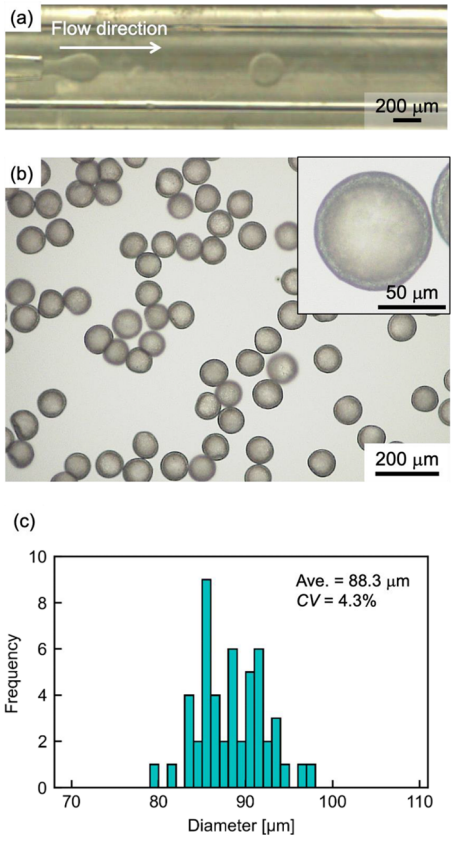

Figure 3. (a) Digital microscopy image of O/W emulsion droplet formation in a microfluidic device. (b) Optical microscopy image of CA microcapsules encapsulating HD. The MCs were prepared at Q_d = 20 μL min^{-1} and Q_c = 600 μL min^{-1}. The inset is a magnified image of a microcapsule showing a core−shell structure. (c) Histogram of the particle size distribution (N = 50).

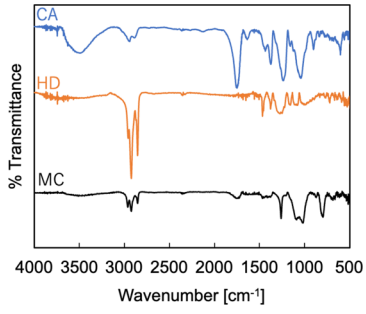

Figure 4. FT-IR spectra of CA, HD, and MCs encapsulating HD (MC).

cm^{-1} due to the asymmetric deformation peak of the $-CH_2-$ group and the symmetric deformation peak of the $-CH_3$ group, respectively. These absorption peaks indicate that CA microcapsules encapsulating HD were successfully obtained.

These results indicate that the equilibrium structure of the droplets after phase separation can be predicted using the spreading coefficient theory and that this fabrication process can be used to continuously produce monodisperse CA microcapsules encapsulating HD in the core.

Thermal Stability Analysis of Microcapsules Encapsulating PCMs

To utilize microcapsules for latent heat storage, the decomposition temperature of the shell polymer must be

https://doi.org/10.1021/acsmaterialsau.1c00068
ACS Mater. Au 2022, 2, 250−259

higher than the boiling point of the encapsulated PCMs. Figure 5 shows the TGA curves of the raw HD, neat CA, and CA

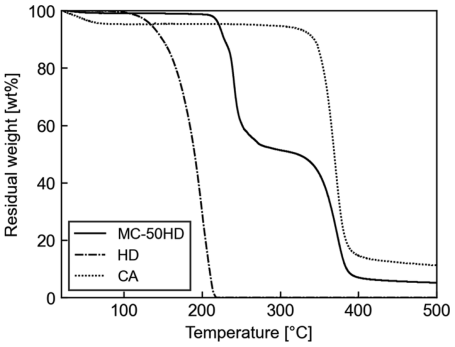

Figure 5. TGA curves of raw HD, neat CA, and CA microcapsules encapsulating HD (MC-50HD). MC-50HD, HD, and CA indicate microcapsules with hexadecane content at 50 wt %, hexadecane, and cellulose acetate, respectively.

microcapsules encapsulating HD. Upon heating, HD evaporated at 150−220 °C. The shell material, CA, lost 2% of its weight at lower than 100 °C due to the evaporation of adsorbed water and then degraded at 360−400 °C. These results clearly show that the thermal stability of CA is higher than that of HD and that CA is thus suitable as a shell material to encapsulate HD. In the case of CA microcapsules, the encapsulated HD disappeared at 230−300 °C, which is significantly higher than the boiling point of raw HD. In addition, CA decomposed at 360−400 °C. These results indicate that the microencapsulation of HD retards the evaporation of HD because of the presence of the shell covering with HD. The HD/CA mass ratio in the microcapsules was approximately 47/53, which is in good agreement with the feed composition.

Effects of the HD Content on the Morphology and Thermal Properties of Microcapsules

To investigate the effects of the HD content on the morphology and thermal properties of microcapsules, microcapsules with different HD contents (33, 40, 50, and 67 wt % as theoretical values) were prepared while maintaining the flow rates constant at Q_d = 20 μL min^{-1} and Q_c = 1000 μL min^{-1}. The sample names are denoted as MC-xHD for x wt % HD in the microcapsules on a feed basis. TGA measurements showed that the HD contents in microcapsules were in good agreement with the theoretical values (Figures S1−S3 and Table S2). Figure 6 shows the SEM images of the surface and cross sections of the microcapsules with different HD contents. Regardless of the HD content, monodisperse microcapsules with a dimpled surface were obtained, and their cross sections had a porous structure. The formation of the porous shell could be due to rapid precipitation of CA during phase separation of the emulsion droplets and the fact that tiny HD droplets did not migrate to the large core, generating the pores after freeze-drying of the samples. As the HD content increased from 33 to 66 wt %, the shell thickness of the microcapsules decreased from 7.3 to 2.7 μm, while the diameter of the microcapsules was increased due to the increase in the volume of HD (Table 3). This result indicates that the shell thickness can be tuned by varying the HD content in the dispersed phase during the fabrication process. It is also noted that the diameter and shell thickness of the resulting microcapsules

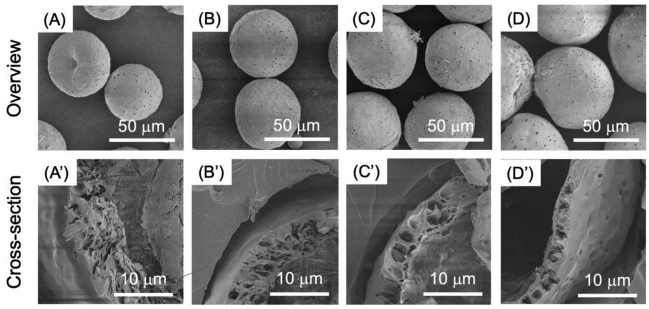

Figure 6. SEM images of HD-encapsulated microcapsules with different HD contents of (A,A′) 33, (B,B′) 40, (C,C′) 50, and (D,D′) 67 wt %. The MCs were prepared at Q_d = 20 μL min^{-1} and Q_c = 1000 μL min^{-1}.

tended to be larger than their theoretical values calculated based upon the droplet diameter and the initial composition of the dispersed phase. This would be due to rapid precipitation of CA during the phase separation, as discussed above.

The thermal properties of raw HD and HD-encapsulated microcapsules with different HD contents, including the onset crystallization temperature (T_{oc}), latent heat capacity during the solidification process (ΔH_c), onset melting temperature (T_{om}), and latent heat capacity during the melting process (ΔH_m), were analyzed by DSC measurements (Figure 7); the specific experimental data are listed in Table 4. There are two peaks in the solidification process, and the major and minor temperature peaks are denoted as (H) and (L), respectively, as shown in Table 4. The main crystallization temperatures (T_{oc} (H)) of MC-33HD, MC-40HD, MC-50HD, and MC-67HD were 15.1, 15.6, 15.6, and 15.2 °C, respectively, which were consistent with that of raw HD (15.5 °C). The latent heat capacity of raw HD during the solidification process was 251 J g^{-1}, and that of MCs increased from 49 to 158 J g^{-1} as the HD content increased. This result indicates that HD encapsulated in microcapsules serves as an energy storage material that absorbs and releases energy through the solid−liquid phase change and that a higher HD content is preferable to increase the latent heat capacity of microcapsules. However, all types of microcapsules show a minor crystallization peak at a low temperature of approximately 2.5 °C, indicating supercooling. This may be attributed to the presence of tiny HD droplets of approximately 1 μm diameter in the shell of the microcapsules, as shown in Figure 6.

Although it is reasonable to evaluate the latent heat storage capacity of microcapsules based on Joules per 1 g of the microcapsules (J (g capsule)$^{-1}$) in the industrial field, as discussed above, Okubo et al. reported that the latent heat storage capacity of the encapsulated wax was decreased when the core and the shell were not completely separated, and this phenomenon can be confirmed by evaluating the latent heat storage capacity in the relative form as Joules per 1 g of encapsulated HD of the microcapsules, which is important from an academic aspect.[28,38] We then evaluated the heat storage capacity of HD encapsulated in the microcapsules based on ΔH^*_c and ΔH^*_m expressed in Joules per 1 g of encapsulated HD as shown in Table S3. The ΔH^*_c and ΔH^*_m values of the encapsulated HD in microcapsules except for MC-67HD were significantly lower than those of pure HD, and the ΔH^*_c and ΔH^*_m values tended to increase and approach those of pure HD with increasing the HD content in the microcapsules. Among those that we tested, only in the

https://doi.org/10.1021/acsmaterialsau.1c00068
ACS Mater. Au 2022, 2, 250−259

Table 3. Characterization of Microcapsules Prepared with Different HD Contents

sample	HD content[a] [wt %]	D_{drop}[b] [μm]	$D_{capsule}$[c] [μm]	CV[d] [%]	$D_{capsule,theoretical}$[e] [μm]	T_{shell}[f] [μm]	$T_{shell,theoretical}$[g] [μm]
MC-33HD	33	196	52	11.3	45	7.3	4.8
MC-40HD	40	201	54	10.9	49	6.4	4.1
MC-50HD	47	199	62	6.1	52	5.1	3.1
MC-67HD	66	204	64	4.4	63	2.7	1.9

[a]Measured with TGA. [b]D_{drop}: droplet diameter. [c]$D_{capsule}$: diameter of microcapsules. [d]CV: coefficient of variance of microcapsules. [e]$D_{capsule,theoretical}$: theoretical diameter of microcapsules calculated from the initial droplet diameter and compositions. [f]T_{shell}: shell thickness of microcapsules. [g]$T_{shell,theoretical}$: theoretical shell thickness calculated from the initial droplet diameter and compositions.

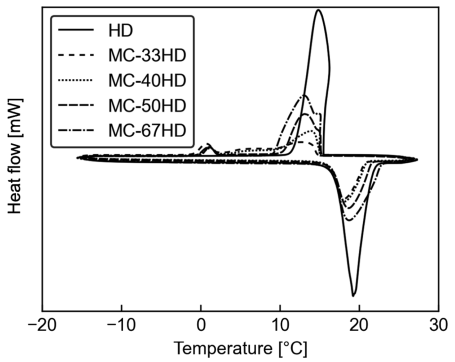

Figure 7. Effect of the HD content on the thermal properties of the microcapsules. HD and MC-*x*HD denote hexadecane and microcapsules encapsulating *x*% hexadecane, respectively.

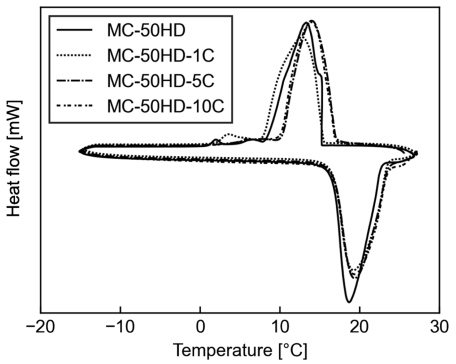

Figure 8. Effect of the concentration of HD-OH on the thermal properties of the microcapsules. The HD content in the microcapsules was fixed at 50 wt %. The sample names are denoted as MC-50HD-*y*C for *y* wt % HD-OH relative to the amount of HD.

Table 4. DSC Data of the Raw HD and HD-Encapsulated Microcapsules with Different HD Contents

sample	HD content [wt %]	T_{oc} (H) [°C]	ΔH_c (H) [J g^{-1}]	T_{oc} (L) [°C]	ΔH_c (L) [J g^{-1}]	T_{om} [°C]	ΔH_m [J g^{-1}]
HD		15.5	251			17.1	251
MC-33HD	33	15.1	49	2.4	11	16.0	75
MC-40HD	40	15.6	70	2.5	7	16.3	87
MC-50HD	47	15.6	96	2.5	9	16.4	112
MC-67HD	66	15.2	158	2.4	8	16.6	165

case of MC-67HD, the ΔH^*_c and ΔH^*_m values of the encapsulated HD were the same as those of the pure one. These results indicate that encapsulating HD in the CA shell does not always result in the same thermal properties of pure HD probably due to the supercooling phenomenon and that the increase in the HD content encapsulated in the microcapsules can reduce the loss of heat storage capacity for pure HD.

Effects of the Presence of a Nucleating Reagent on the Thermal Properties and Morphology of the Microcapsules

To mitigate the supercooling phenomenon in HD encapsulated in the microcapsules, 1-hexadecanol (HD-OH) was introduced as a nucleating reagent in the dispersed phase,[40] and HD-encapsulated microcapsules with different HD-OH concentrations (1, 5, and 10 wt % relative to the mass of HD) were prepared using the same procedure. Figure 8 shows the DSC thermograms of the microcapsules with different concentrations of HD-OH, and the analyzed data are summarized in Table 5. The sample names are denoted as MC-50HD-*y*C for *y* wt % HD-OH relative to the amount of HD. Comparing the thermal properties of HD-encapsulated microcapsules with 1 wt % and without HD-OH, the microcapsules with 1 wt % HD-OH had a higher latent heat capacity of HD during the crystallization process than those without HD-OH and did not exhibit the minor crystallization peak at approximately 2 °C. In addition, a further increase in the concentration of HD-OH from 1 to 5 or 10 wt % facilitated the crystallization of HD and narrowed the width of the crystallization peak while maintaining a constant latent heat capacity of approximately 105−111 J g^{-1}. The onset temperature of the main crystallization peak (T_{oc} (H)) of the microcapsules with more than 5 wt % HD-OH was approximately 1 °C higher than that of the microcapsules with less than 1 wt % HD-OH and neat HD. These results indicate that HD-OH serves as a nucleating reagent in the crystallization process and facilitates the crystallization of HD encapsulated in the microcapsules. The mitigation of the supercooling phenomenon could be derived from heterogeneous nucleation.[41−43] HD-OH is a hydrophobic alcohol with a higher crystallization temperature than HD and could be soluble in HD encapsulated in microcapsules. Therefore, during the cooling process of the microcapsules, HD-OH dissolved in HD first becomes a solid state, which could play a role in the nuclei to proceed with the crystallization of HD.

Figure 9 shows the SEM images of microcapsules with different concentrations of HD-OH. Regardless of the concentration of HD-OH, there were no significant differences in the morphology and shell structure of the microcapsules, and the shell had a porous structure. The diameter and shell thickness of the microcapsules tended to be larger than the theoretical ones due to the rapid precipitation of CA during solvent diffusion and porous shell formation (Table 6). This indicates that the introduction of HD-OH in the dispersed phase contributes to the mitigation of the supercooling phenomenon of HD encapsulated in the microcapsules but

https://doi.org/10.1021/acsmaterialsau.1c00068
ACS Mater. Au 2022, 2, 250−259

Table 5. DSC Data of the Raw HD and HD-Encapsulated Microcapsules with Different Concentrations of HD-OH[a]

sample	$C_{HD\text{-}OH}$ [wt %]	T_{oc} (H) [°C]	ΔH_c (H) [J g^{-1}]	T_{oc} (L) [°C]	ΔH_c (L) [J g^{-1}]	T_{om} [°C]	ΔH_m [J g^{-1}]
HD		15.5	251			17.1	251
MC-50HD	0	15.6	96	2.5	9	16.4	112
MC-50HD-1C	1	15.8	111			16.7	113
MC-50HD-5C	5	16.9	105			16.9	107
MC-50HD-10C	10	16.8	110			16.7	110

[a]The HD content in the microcapsules was fixed at 50 wt %.

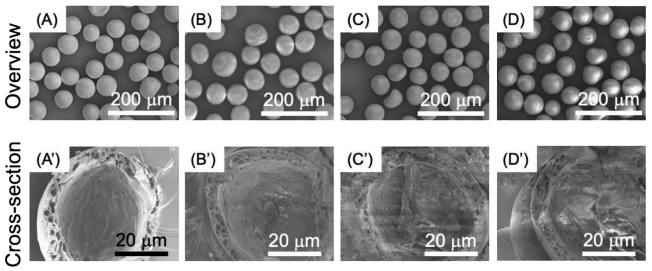

Figure 9. SEM images of HD-encapsulated microcapsules with different concentrations of HD-OH of (A,A′) 0, (B,B′) 1, (C,C′) 5, and (D,D′) 10 wt %, relative to the amount of HD. The HD content in the microcapsules was fixed at 50 wt %.

does not affect the shell structure. In general, when introducing a nucleating reagent to the microcapsules for latent heat applications, the mass content of the nucleation agent must be minimal to keep the latent heat capacity as high as possible. In the following experiment, the concentration of HD-OH was fixed at 5 wt % relative to the weight of HD.

Effects of the Cross-Linker on the Morphology and the Thermal Properties of the Microcapsules

To prepare CA microcapsules with a dense shell, we added PPG-TDI as a cross-linker to the shells of the CA microcapsules. Because CA microcapsules could be cross-linked via the reaction of the OH group of CA with the isocyanate group of PPG-TDI, the resulting cross-linked CA microcapsules formed a dense shell network analogous to the case of electrospun PEG/CA nanofibers.[44] Here, we prepared HD-encapsulated microcapsules with different PPG-TDI concentrations (0, 0.2, 0.4, and 0.6 wt % relative to the mass of the dispersed phase) and fixed amounts of HD and HD-OH using the same procedure and evaluated their morphology and thermal properties.

Figure 10 shows the FT-IR spectra of PPG-TDI, CA microcapsules encapsulating HD, and cross-linked CA microcapsules encapsulating HD. For both PPG-TDI and cross-linked CA microcapsules, the characteristic peaks at 2270 cm^{-1} due to the N═C═O bands, at 1600 cm^{-1} due to the stretching vibration of the C═C group, and at 1521 cm^{-1} due to the stretching vibration of the C═O group were confirmed.

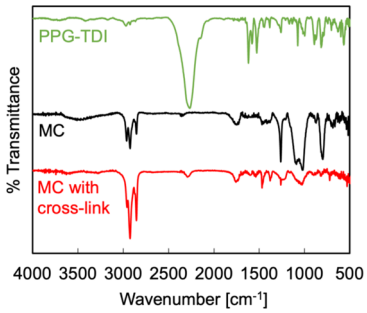

Figure 10. FT-IR spectra of PPG-TDI, MCs encapsulating HD (MC), and cross-linked MCs encapsulating HD (MC with cross-linking).

In addition, for cross-linked CA microcapsules, the characteristic broad peak in the region of 3200−3400 cm^{-1} due to the stretching vibration of the −NH group was confirmed. These results indicate that PPG-TDI was successfully incorporated in the shell of the CA microcapsules.

Figure 11 shows the SEM images of the cross-linked CA microcapsules with different concentrations of PPG-TDI. As

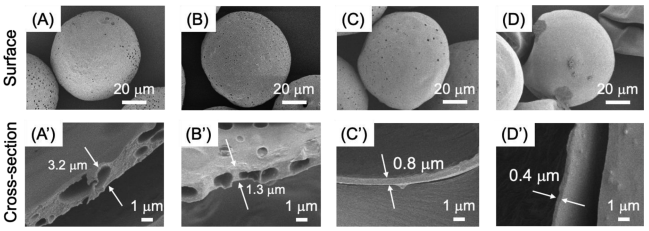

Figure 11. SEM images of HD-encapsulated microcapsules with different concentrations of the cross-linker. The concentrations of PPG-TDI were (A,A′) 0, (B,B′) 0.2, (C,C′) 0.4, and (D,D′) 0.6 wt %, relative to the total amount of the dispersed phase.

the concentration of PPG-TDI increased, the number of dimples on the surface of the microcapsules tended to decrease, while the diameter of the microcapsules tended to increase (Table 7). In addition, the shell thickness of the microcapsules significantly decreased with increasing the

Table 6. Characterization of Microcapsules Prepared with Different Concentrations of HD-OH

sample	$C_{HD\text{-}OH}$[a] [wt %]	D_{drop}[b] [μm]	$D_{capsule}$[c] [μm]	CV[d] [%]	$D_{capsule,theoretical}$[e] [μm]	T_{shell}[f] [μm]	$T_{shell,theoretical}$[g] [μm]
MC-50HD	0	199	62	6.1	52	5.1	3.1
MC-50HD-1C	1	199	62	5.4	52	5.5	3.1
MC-50HD-5C	5	204	65	6.0	54	5.0	3.1
MC-50HD-10C	10	203	65	6.2	54	6.2	3.0

[a]$C_{HD\text{-}OH}$: concentration of HD-OH relative to the mass of HD. [b]D_{drop}: droplet diameter. [c]$D_{capsule}$: diameter of microcapsules. [d]CV: coefficient of variance of microcapsules. [e]$D_{capsule,theoretical}$: theoretical diameter of microcapsules calculated from the initial droplet diameter and compositions. [f]T_{shell}: shell thickness of microcapsules. [g]$T_{shell,theoretical}$: theoretical shell thickness calculated from the initial droplet diameter and compositions.

https://doi.org/10.1021/acsmaterialsau.1c00068
ACS Mater. Au 2022, 2, 250−259

Table 7. Characterization of Microcapsules Prepared with Different Concentrations of PPG-TDI

sample	$C_{PPG\text{-}TDI}$[a] [wt %]	D_{drop}[b] [μm]	$D_{capsule}$[c] [μm]	CV[d] [%]	$D_{capsule,theoretical}$[e] [μm]	T_{shell}[f] [μm]	$T_{shell,theoretical}$[g] [μm]
MC-67HD-5C	0	207	77	6.0	65	3.2	1.9
MC-67HD-5C-0.2CL	0.2	207	80	7.9	65	1.3	2.4
MC-67HD-5C-0.4CL	0.4	201	87	7.1	64	0.8	2.8
MC-67HD-5C-0.6CL	0.6	216	89	6.1	70	0.4	3.6

[a]$C_{PPG\text{-}TDI}$: concentration of PPG-TDI relative to the mass of the dispersed phase. [b]D_{drop}: droplet diameter. [c]$D_{capsule}$: diameter of microcapsules. [d]CV: coefficient of variance of microcapsules. [e]$D_{capsule,theoretical}$: theoretical diameter of microcapsules calculated from the initial droplet diameter and compositions. [f]T_{shell}: shell thickness of microcapsules. [g]$T_{shell,theoretical}$: theoretical shell thickness calculated from the initial droplet diameter and compositions.

concentration of PPG-TDI, which resulted in the formation of a dense and thin shell when the concentration was equal to or larger than 0.4 wt % relative to the mass of the dispersed phase. We have not elucidated the detailed mechanism by which PPG-TDI serves to prevent the formation of a porous shell; however, PPG-TDI may facilitate the phase separation of CA/PPG-TDI-rich and HD/HD-OH-rich phases. The increase in microcapsule size cannot be simply explained by the increase in the volume due to an increase in the amount of PPG-TDI added, but it can be attributed to the formation of a skin layer during solvent diffusion and the subsequent deformation of the microcapsules in a constant volume. These results indicate that cross-linking of the CA microcapsules using PPG-TDI can be effective to form microcapsules with a dense and thin shell.

Figure 12 shows the DSC thermograms of the cross-linked CA microcapsules with different concentrations of PPG-TDI,

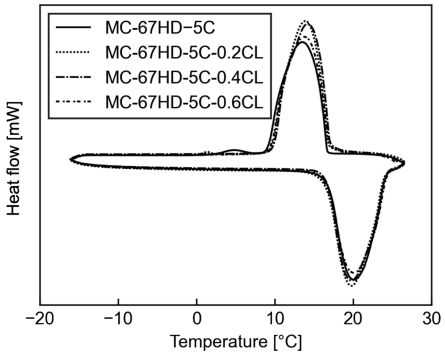

Figure 12. Effect of the concentration of PPG-TDI on the thermal properties of the microcapsules. The HD content in the microcapsules was fixed at 67 wt %. The concentration of HD-OH relative to the amount of HD was fixed at 5 wt %. The sample names are denoted as MC-67HD-5C-*z*CL for *z* wt % PPG-TDI relative to the total weight of the dispersed phase.

Table 8. DSC Data of the Raw Commercial HD and HD-Encapsulated Microcapsules with Different Concentrations of PPG-TDI[a]

sample	$C_{PPG\text{-}TDI}$ [wt %]	T_{oc} (H) [°C]	ΔH_c (H) [J g^{-1}]	T_{om} [°C]	ΔH_m [J g^{-1}]
HD		15.5	251	17.1	251
MC-67HD-5C	0	17.8	161	16.8	160
MC-67HD-5C-0.2CL	0.2	18.7	176	16.7	178
MC-67HD-5C-0.4CL	0.4	18.5	176	16.9	178
MC-67HD-5C-0.6CL	0.6	18.3	172	16.7	171

[a]The concentration of PPG-TDI was relative to the total weight of the dispersed phase.

and the analyzed data are summarized in Table 8. The sample names are denoted as MC-67HD-5C-*z*CL for *z* wt % PPG-TDI relative to the total mass of the dispersed phase. Comparing the thermal properties of HD-encapsulated microcapsules with and without PPG-TDI, the microcapsules with PPG-TDI had a higher latent heat storage capacity of HD upon crystallization than those without PPG-TDI. As the concentration of PPG-TDI was increased from 0 to 0.4 wt %, the latent heat storage capacity tended to increase from 161 to 176 J g^{-1}; however, as the concentration was further increased to 0.6 wt %, it slightly decreased to 172 J g^{-1}. Because of the presence of HD-OH in the microcapsules, there were no clear differences in the shapes of the DSC curves among the four samples, and no supercooling phenomenon was detected. Based on these results, we showed that cross-linked CA microcapsules with HD-OH as a nucleation reagent had a core−shell structure with a dense and thin shell and exhibited an excellent latent heat storage capacity of up to 176 J g^{-1} without any supercooling phenomenon.

To confirm the thermal stability of the microcapsules, the thermal cycling test was performed 50 times in the temperature range of −10 to 30 °C (Figure 13). It is noted that the

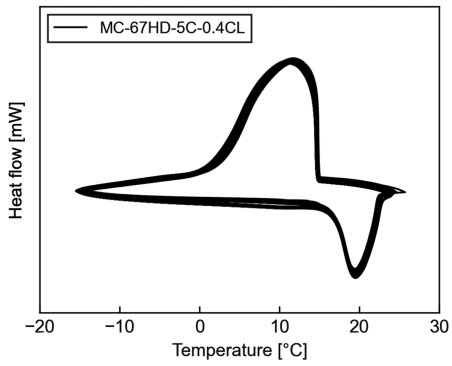

Figure 13. Thermal cyclic tests of the microcapsules encapsulating HD. The sample experienced 50 cooling/heating cycles at 5 °C min^{-1}.

cooling/heating rate on this measurement was set at 5 °C min^{-1}, which is 5 times higher than the other DSC measurements in this study. The DSC curves for the first cycle and the 50th cycle were in good agreement, and there were no significant changes in the values of ΔH_c and ΔH_m in each step (Figure S4 and Table 9), although the heat storage capacities of the sample were lower than those of samples in Table 8 probably due to occurrence of the supercooling phenomenon of the encapsulated HD by the higher cooling/heating rate. These results suggest that the microcapsules have

https://doi.org/10.1021/acsmaterialsau.1c00068
ACS Mater. Au 2022, 2, 250−259

Table 9. Latent Heat Capacity of the HD-Encapsulated Microcapsules after the 1st and 50th Thermal Cyclic Tests

	ΔH_c [J g^{-1}]		ΔH_m [J g^{-1}]	
sample	1st cycle	50th cycle	1st cycle	50th cycle
MC-67HD-5C-0.4CL	136	138	130	130

good thermal reliability in the temperature range of −10 and 30 °C.

CONCLUSIONS

We developed a continuous microflow process to prepare monodisperse CA microcapsules encapsulating HD in the core for latent heat storage applications by combining microfluidic droplet formation with subsequent solvent removal from the droplets through solvent diffusion. The latent heat storage capacity of the encapsulated HD increased as the content of HD in the microcapsules increased. The supercooling of encapsulated HD in the microcapsules was eliminated by adding HD-OH to the microcapsules, and the cross-linking of the CA shell with PPG-TDI resulted in the formation of a thin and dense shell. The resulting CA microcapsules with a dense and thin shell showed a latent heat storage capacity of 176 J g^{-1} without a supercooling phenomenon. Thermal cyclic tests of the microcapsules showed a negligible decrease in the latent heat capacity after experiencing 50 cooling/heating cycles. This result indicates that the microcapsules have good thermal reliability. Therefore, we expect that the prepared CA microcapsules are a potential candidate for storage media in thermal energy storage systems. Further study will be needed to develop a mass production system of the microcapsules by numbering up of the devices as well as to evaluate the thermal energy storage behavior in practical use such as real-time infrared thermographic analysis and temperature control of the environment.

ASSOCIATED CONTENT

Supporting Information

The Supporting Information is available free of charge at https://pubs.acs.org/doi/10.1021/acsmaterialsau.1c00068.

Characteristics of the dispersed phases; TGA curves of raw HD, neat CA, and HD-encapsulated CA microcapsules (MC-33HD, MC-40HD, and MC-67HD); compositions of microcapsules encapsulating HD; DSC data of the HD content in the microcapsules and latent heats of the encapsulated HD in the microcapsules; change in the latent heat storage capacity of the microcapsules during thermal cyclic tests (sample: MC-67HD-5C-0.4CL) (PDF)

AUTHOR INFORMATION

Corresponding Authors

Takaichi Watanabe − *Department of Applied Chemistry, Graduate School of Natural Science and Technology, Okayama University, Okayama 700-8530, Japan;* orcid.org/0000-0002-5855-2583; Phone: +81-86-251-8072; Email: wata-t@okayama-u.ac.jp

Tsutomu Ono − *Department of Applied Chemistry, Graduate School of Natural Science and Technology, Okayama University, Okayama 700-8530, Japan;* orcid.org/0000-0002-2880-7119; Phone: +81-86-251-8083; Email: tono@okayama-u.ac.jp

Authors

Yuko Sakai − *Department of Applied Chemistry, Graduate School of Natural Science and Technology, Okayama University, Okayama 700-8530, Japan*

Naomi Sugimori − *Chusei Oil Co., Ltd., Kurashiki 713-8103, Japan*

Toshinori Ikeda − *Chusei Oil Co., Ltd., Kurashiki 713-8103, Japan*

Masayuki Monzen − *Chusei Oil Co., Ltd., Kurashiki 713-8103, Japan*

Complete contact information is available at: https://pubs.acs.org/10.1021/acsmaterialsau.1c00068

Author Contributions

T.W. and T.O. designed the experiments. T.W., Y.S., and N.S. performed all the experiments, and T.W., Y.S., N.S., and T.I. analyzed the data. T.W., Y.S., and N.S. interpreted the results. T.W. wrote the manuscript. T.W., M.M., and T.O. designed the study.

Notes

The authors declare no competing financial interest.

ACKNOWLEDGMENTS

This work was supported by a grant from the METI Monozukuri R&D Support Grant Program for SMEs (Grant Number JPJ005698).

REFERENCES

(1) Liu, H.; Wang, X.; Wu, D. Innovative Design of Microencapsulated Phase Change Materials for Thermal Energy Storage and Versatile Applications: a Review. *Sustainable Energy Fuels* **2019**, *3*, 1091−1149.

(2) Li, J.; Sun, Y. Z.; Liu, H.; Wang, X. Innovative Integration of Phase-Change Microcapsules with Metal−Organic Frameworks into an Intelligent Biosensing System for Enhancing Dopamine Detection. *ACS Appl. Mater. Interfaces* **2021**, *13*, 41753−41772.

(3) Yu, J.; Liu, H.; Wang, Y.; Li, J.; Wu, D.; Wang, X. Fluorescent Sensing System based on Molecularly Imprinted Phase-Change Microcapsules and Carbon Quantum Dots for High-Efficient Detection of Tetracycline. *J. Colloid Interface Sci.* **2021**, *599*, 332−350.

(4) Su, J.-F.; Wang, L.-X.; Ren, L. Synthesis of Polyurethane MicroPCMs Containing N-Octadecane by Interfacial Polycondensation: Influence of Styrene-Maleic Anhydride as a Surfactant. *Colloids Surf., A* **2007**, *299*, 268−275.

(5) Yang, Y.; Xia, R.; Zhao, J.; Shang, L.; Liu, Y.; Guo, H. Preparation and Thermal Properties of Microencapsulated Polyurethane and Double-Component Poly(ethylene Glycol) as Phase Change Material for Thermal Energy Storage by Interfacial Polymerization. *Energy Fuels* **2020**, *34*, 1024−1032.

(6) Cai, C.; Ouyang, X.; Zhou, L.; Liu, G.; Wang, Y.; Zhu, G.; Yao, J.; Militky, J.; Venkataraman, M.; Zhang, G. Co-Solvent Free Interfacial Polycondensation and Properties of Polyurea PCM Microcapsules with Dodecanol Dodecanoate as Core Material. *Solar Energy* **2020**, *199*, 721−730.

(7) Srinivasaraonaik, B.; Singh, L. P.; Tyagi, I.; Rawat, A.; Sinha, S. Microencapsulation of a Eutectic PCM Using in Situ Polymerization Technique for Thermal Energy Storage. *Int. J. Energy Res.* **2020**, *44*, 3854−3864.

(8) Salaün, F.; Devaux, E.; Bourbigot, S.; Rumeau, P. Influence of Process Parameters on Microcapsules Loaded with N-Hexadecane Prepared by in Situ Polymerization. *Chem. Eng. J.* **2009**, *155*, 457−465.

(9) Huang, R.; Li, W.; Wang, J.; Zhang, X. Effects of Oil-Soluble Etherified Melamine-Formaldehyde Prepolymers on: In Situ Microencapsulation and Macroencapsulation of N-Dodecanol. *New J. Chem.* **2017**, *41*, 9424−9437.
(10) Parvate, S.; Singh, J.; Dixit, P.; Vennapusa, J. R.; Maiti, T. K.; Chattopadhyay, S. Titanium Dioxide Nanoparticle-Decorated Polymer Microcapsules Enclosing Phase Change Material for Thermal Energy Storage and Photocatalysis. *ACS. Appl. Polym. Mater.* **2021**, *3*, 1866−1879.
(11) Chaiyasat, P.; Ogino, Y.; Suzuki, T.; Okubo, M. Influence of Water Domain Formed in Hexadecane Core inside Cross-Linked Capsule Particle on Thermal Properties for Heat Storage Application. *Colloid Polym. Sci.* **2008**, *286*, 753−759.
(12) Borreguero, A. M.; Carmona, M.; Sanchez, M. L.; Valverde, J. L.; Rodriguez, J. F. Improvement of the Thermal Behaviour of Gypsum Blocks by the Incorporation of Microcapsules Containing PCMS Obtained by Suspension Polymerization with an Optimal Core/coating Mass Ratio. *Appl. Therm. Eng.* **2010**, *30*, 1164−1169.
(13) Sarı, A.; Alkan, C.; Karaipekli, A. Preparation, Characterization and Thermal Properties of PMMA/n-Heptadecane Microcapsules as Novel Solid−liquid microPCM for Thermal Energy Storage. *Appl. Energy* **2010**, *87*, 1529−1534.
(14) Yin, D.; Ma, L.; Liu, J.; Zhang, Q. Pickering Emulsion: A Novel Template for Microencapsulated Phase Change Materials with Polymer−silica Hybrid Shell. *Energy* **2014**, *64*, 575−581.
(15) Zou, X.; Zhou, W.; Shi, J.; Ye, Y.; Zhao, Y.; Zhang, H.; Liu, Y.; Yu, Y.; Guo, J. Preparation and Characterization of Poly (N-Methylol Acrylamide)/polyethylene Glycol Composite Phase Change Materials for Thermal Energy Storage. *Sol. Energy Mater. Sol. Cells* **2020**, *205*, 110248.
(16) Naikwadi, A. T.; Samui, A. B.; Mahanwar, P. A. Melamine-Formaldehyde Microencapsulated N-Tetracosane Phase Change Material for Solar Thermal Energy Storage in Coating. *Sol. Energy Mater. Sol. Cells* **2020**, *215*, 110676.
(17) Su, J.; Wang, L.; Ren, L. Fabrication and Thermal Properties of microPCMs: Used Melamine-Formaldehyde Resin as Shell Material. *J. Appl. Polym. Sci.* **2006**, *101*, 1522−1528.
(18) Tzavidi, S.; Zotiadis, C.; Porfyris, A.; Korres, D. M.; Vouyiouka, S. Epoxy Loaded Poly (urea-formaldehyde) Microcapsules via in Situ Polymerization Designated for Self-healing Coatings. *J. Appl. Polym. Sci.* **2020**, *137*, 49323.
(19) Han, T.; Wang, X.; Li, D.; Li, D.; Xing, F.; Han, N. Impermeability Characteristics of Cementitious Materials with Self-Healing Based on Epoxy/urea-Formaldehyde Microcapsules Using an Immersion Test. *Constr. Build. Mater.* **2020**, *259*, 119782.
(20) Han, S.; Chen, Y.; Lyu, S.; Chen, Z.; Wang, S.; Fu, F. Effects of Processing Conditions on the Properties of Paraffin/melamine-Urea-Formaldehyde Microcapsules Prepared by in Situ Polymerization. *Colloids Surf., A* **2020**, *585*, 124046.
(21) Brown, E. N.; Kessler, M. R.; Sottos, N. R.; White, S. R. In Situ Poly(urea-Formaldehyde) Microencapsulation of Dicyclopentadiene. *J. Microencapsulation* **2003**, *20*, 719−730.
(22) Yuan, L.; Liang, G.; Xie, J.; Li, L.; Guo, J. Preparation and Characterization of Poly(urea-Formaldehyde) Microcapsules Filled with Epoxy Resins. *Polymer* **2006**, *47*, 5338−5349.
(23) Su, J. F.; Wang, L. X.; Ren, L.; Huang, Z.; Meng, X. W. Preparation and Characterization of Polyurethane Microcapsules Containing N-octadecane with Styrene-maleic Anhydride as a Surfactant by Interfacial Polycondensation. *J. Appl. Polym. Sci.* **2006**, *102*, 4996−5006.
(24) Ma, Y.; Li, Z.; Wang, H.; Li, H. Synthesis and Optimization of Polyurethane Microcapsules Containing [BMIm] PF6 Ionic Liquid Lubricant. *J. Colloid Interface Sci.* **2019**, *534*, 469−479.
(25) Xiong, T.; Shah, K. W.; Kua, H. W. Thermal Performance Enhancement of Cementitious Composite Containing Polystyrene/n-Octadecane Microcapsules: An Experimental and Numerical Study. *Renewable Energy* **2021**, *169*, 335−357.
(26) Döğüşcü, D. K.; Altıntaş, A.; Sarı, A.; Alkan, C. Polystyrene Microcapsules with Palmitic-Capric Acid Eutectic Mixture as Building Thermal Energy Storage Materials. *Energy Build.* **2017**, *150*, 376−382.
(27) Sánchez-Silva, L.; Rodríguez, J. F.; Carmona, M.; Romero, A.; Sánchez, P. Thermal and Morphological Stability of Polystyrene Microcapsules Containing Phase-Change Materials. *J. Appl. Polym. Sci.* **2011**, *120*, 291−297.
(28) Chaiyasat, P.; Noppalit, S.; Okubo, M.; Chaiyasat, A. Innovative Synthesis of High Performance Poly(methyl Methacrylate) Microcapsules with Encapsulated Heat Storage Material by Microsuspension Iodine Transfer Polymerization (ms ITP). *Sol. Energy Mater. Sol. Cells* **2016**, *157*, 996−1003.
(29) Takei, T.; Yamasaki, Y.; Yuji, Y.; Sakoguchi, S.; Ohzuno, Y.; Hayase, G.; Yoshida, M. Millimeter-sized Capsules Prepared Using Liquid Marbles: Encapsulation of Ingredients with High Efficiency and Preparation of Spherical Core-shell Capsules with Highly Uniform Shell Thickness Using Centrifugal Force. *J. Colloid Interface Sci.* **2019**, *536*, 414−423.
(30) Han, X.; Kong, T.; Zhu, P.; Wang, L. Microfluidic Encapsulation of Phase-Change Materials for High Thermal Performance. *Langmuir* **2020**, *36*, 8165−8173.
(31) Dowding, P. J.; Atkin, R.; Vincent, B.; Bouillot, P. Oil Core-Polymer Shell Microcapsules Prepared by Internal Phase Separation from Emulsion Droplets. I. Characterization and Release Rates for Microcapsules with Polystyrene Shells. *Langmuir* **2004**, *20*, 11374−11379.
(32) Lensen, D.; van Breukelen, K.; Vriezema, D. M.; van Hest, J. C. M. Preparation of Biodegradable Liquid Core PLLA Microcapsules and Hollow PLLA Microcapsules Using Microfluidics. *Macromol. Biosci.* **2010**, *10*, 475−480.
(33) Watanabe, T.; Kimura, Y.; Ono, T. Microfluidic Fabrication of Monodisperse Polylactide Microcapsules with Tunable Structures through Rapid Precipitation. *Langmuir* **2013**, *29*, 14082−14088.
(34) Zhang, S.; Campagne, C.; Salaün, F. Preparation of N-Alkane/Polycaprolactone Phase-Change Microcapsules via Single Nozzle Electro-Spraying: Characterization on Their Formation, Structures and Properties. *Appl. Sci.* **2020**, *10*, 561.
(35) Feczkó, T.; Kardos, A. F.; Németh, B.; Trif, L.; Gyenis, J. Microencapsulation of N-Hexadecane Phase Change Material by Ethyl Cellulose Polymer. *Polym. Bull.* **2014**, *71*, 3289−3304.
(36) Lin, Y.; Zhu, C.; Alva, G.; Fang, G. Microencapsulation and Thermal Properties of Myristic Acid with Ethyl Cellulose Shell for Thermal Energy Storage. *Appl. Energy* **2018**, *231*, 494−501.
(37) Watanabe, T.; Motohiro, I.; Ono, T. Microfluidic Formation of Hydrogel Microcapsules with a Single Aqueous Core by Spontaneous Cross-Linking in Aqueous Two-Phase System Droplets. *Langmuir* **2019**, *35*, 2358.
(38) Chaiyasat, P.; Noppalit, S.; Okubo, M.; Chaiyast, A. Do Encapsulated Heat Storage Materials Really Retain Their Original Thermal Properties? *Phys. Chem. Chem. Phys.* **2015**, *17*, 1053−1059.
(39) Torza, S.; Mason, S. G. Coalescence of Two Immiscible Liquid Drops. *Science* **1969**, *163*, 813−814.
(40) Zhang, Z.; Yuan, Y.; Zhang, N.; Cao, X. Experimental Investigation on Thermophysical Properties of Capric Acid−lauric Acid Phase Change Slurries for Thermal Storage System. *Energy* **2015**, *90*, 359−368.
(41) Zahir, M. H.; Mohamed, S. A.; Saidur, R.; Al-Sulaiman, F. A. Supercooling of Phase-Change Materials and the Techniques Used to Mitigate the Phenomenon. *Appl. Energy* **2019**, *240*, 793−817.
(42) Zhang, X.-X.; Fan, Y.-F.; Tao, X.-M.; Yick, K.-L. Crystallization and Prevention of Supercooling of Microencapsulated N-Alkanes. *J. Colloid Interface Sci.* **2005**, *281*, 299−306.
(43) Al-Shannaq, R.; Kurdi, J.; Al-Muhtaseb, S.; Dickinson, M.; Farid, M. Supercooling Elimination of Phase Change Materials (PCMs) Microcapsules. *Energy* **2015**, *87*, 654−662.
(44) Chen, C.; Wang, L.; Huang, Y. Crosslinking of the Electrospun Polyethylene Glycol/cellulose Acetate Composite Fibers as Shape-Stabilized Phase Change Materials. *Mater. Lett.* **2009**, *63*, 569−571.

https://doi.org/10.1021/acsmaterialsau.1c00068
ACS Mater. Au 2022, 2, 250−259